Journal of Photonics for Energy

PhotonicsforEnergy.SPIEDigitalLibrary.org

# Index-tunable terahertz metamaterials based on double-layered closed-ring resonator arrays

Yuki Watanabe
Tatsunosuke Matsui

SPIE.

Yuki Watanabe, Tatsunosuke Matsui, "Index-tunable terahertz metamaterials based on double-layered closed-ring resonator arrays," *J. Photon. Energy* **8**(3), 032211 (2018), doi: 10.1117/1.JPE.8.032211.

# Index-tunable terahertz metamaterials based on double-layered closed-ring resonator arrays

**Yuki Watanabe[a] and Tatsunosuke Matsui[a,b,*]**
[a]Mie University, Department of Electrical and Electronic Engineering, Graduate School of Engineering, Tsu, Mie, Japan
[b]Mie University, Center of Ultimate Technology on Nano-Electronics, Tsu, Mie, Japan

**Abstract.** We demonstrate index-tunable metamaterials working in the terahertz (THz) frequency range based on double-layered closed-ring resonator (CRR) arrays. The double-layered CRR arrays have a narrow-band transmission peak in a relatively wide stop band, and that peak shows spectral shift by slightly shifting relative position of the arrays or changing dielectric constant of the dielectric media inserted between CRR arrays. We show by numerical simulations that the effective refractive index can be widely tuned from un-naturally high positive to near-zero and negative values. Our approach may be utilized to develop THz active devices.
 [DOI: 10.1117/1.JPE.8.032211]

**Keywords:** metamaterials; terahertz; closed-ring resonator; refractive index; numerical simulation.

Paper 18025SS received Feb. 6, 2018; accepted for publication Apr. 3, 2018; published online May 3, 2018.

## 1 Introduction

Research on terahertz (THz) science and technology has made significant progress in recent years.[1,2] The THz frequency range is generally considered to be the range of 0.1 to 10 THz and electromagnetic (EM) waves that fall in the THz range can be utilized for various types of applications, such as spectroscopy, nondestructive inspection, security, information, and communications technology. To accelerate research and development of THz technology, development of optical devices based on metamaterial concepts has been extensively studied in recent years.[3,4]

Metamaterials are artificial materials, which show exotic functionality not found in nature.[5–7] In the early stage of the metamaterial research, studies focused on the field of optics and optical effects, such as negative refraction[8] and superlensing,[9–11] were actively studied. To realize such functionalities, subwavelength resonant structures such as split-ring resonators (SRRs)[12] have been invented. SRRs can even resonantly interact with the magnetic field of EM waves and yield functionalities, such as negative magnetic permeability. However, such metamaterials based on subwavelength resonant elements, or "meta-atoms," can only function at certain frequencies determined by their geometrical parameters. One area of intense interest in order to develop next generation of metamaterials and metadevices is active tuning of metamaterials as well as expanding their working frequency range.

Many approaches have been explored to make active metamaterials and metadevices. Various methods to make a relative displacement between closely placed pair of meta-atoms or pair of metasurfaces have been reported.[13–24] When two (or more) meta-atoms are placed close enough to couple via near-field interactions, new resonant modes can be supported akin to bonding and antibonding molecular orbitals in molecular systems. These new resonant modes are quite sensitive to the relative position and/or orientation of meta-atoms and therefore can give

*Address all correspondence to: Tatsunosuke Matsui, E-mail: matsui@elec.mie-u.ac.jp

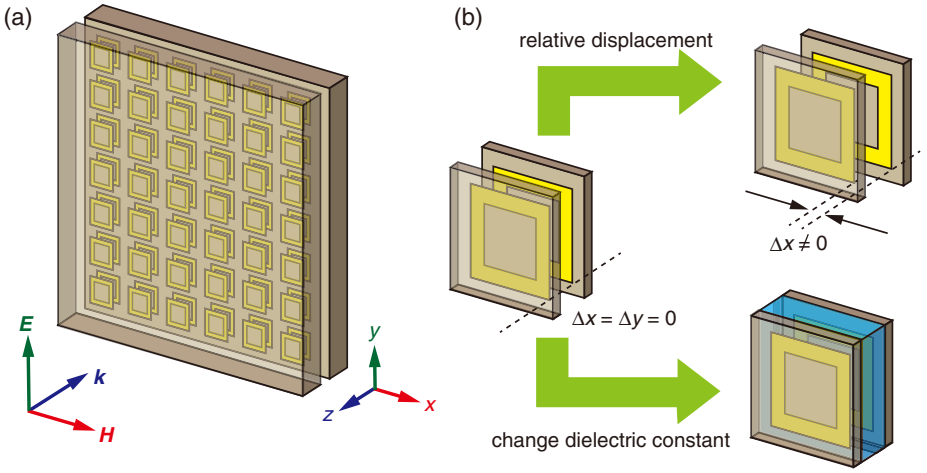


**Fig. 1** Schematic representation of (a) the structure of a double-layered CRR array and (b) the operating principles of an index-tunable THz metamaterial. Tunability is achieved by shifting the relative position or changing the dielectric constant of a spacer layer inserted between two CRR arrays.

a mechanism to tune the resonant frequency by giving a relative displacement. Similar mechanisms can apply to layered arrays of meta-atoms or metasurfaces. Recently, such active tuning has been experimentally realized by slightly shifting relative position of double-layered metamaterials utilizing $\pi$-conjugated polymer actuators,[22] MEMS actuators,[23] or microcantilever.[24] We recently demonstrated that double-layered closed-ring resonator (CRR) arrays are capable of relatively large tuning.[25,26] A paired CRR THz metamaterial was first proposed by Gu et al.[27] to show resonant responses and a negative refractive index even in normal incidence. Based on their basic concept in the double-layered CRR array structure, we have expanded on the idea to realize tuning of resonant responses by shifting relative position of the arrays or by changing dielectric constant of the dielectrics inserted between two layers.[25,26] The operative principle of our device is schematically shown in Fig. 1. Here, we further show that double-layered CRR arrays offer another tuning capability, not only in their resonant frequency but also in the effective refractive index in a wide range from positive high to near-zero and negative values. Negative magnetic permeability,[12] negative refractive index, and negative refraction[8,9] were epoch-making topics in the early stage of metamaterials research. Recent progress further shows that metamaterials offer great potential to develop optical materials and components with an un-naturally high refractive index[28–30] and even near-zero index.[31,32] Our approach may be utilized to develop types of THz active devices.

## 2 Modeling, Numerical Simulation, and Parameter Retrieval

In this study, modeling of the devices and analysis of their THz responses were performed using three-dimensional (3-D) EM field analysis software, CST Microwave Studio (Computer Simulation Technology Inc.). The effective refractive indices were retrieved from the analyzed complex scattering coefficients. This section describes the procedures for these analyses.

### 2.1 *Modeling of Double-Layered Closed-Ring Resonator Arrays*

In our model, we assume that periodic arrays of CRR made of aluminum are placed on quartz substrate. Here, we chose aluminum in accordance with a previous report by Gu et al.[27] We also did similar simulation with copper and gold, however, not much difference was seen in the obtained spectra (data are not shown). The unit cell of designed CRR arrays and the polarization direction of the incident EM field are shown in Fig. 2(a). The side length $L$ and width $W$ of each CRR are 80 and 5 $\mu$m, respectively, and they are periodically arranged with the spacing $A$ between adjacent CRRs in the same array to be 25 $\mu$m in both $x$ and $y$ directions. The thickness

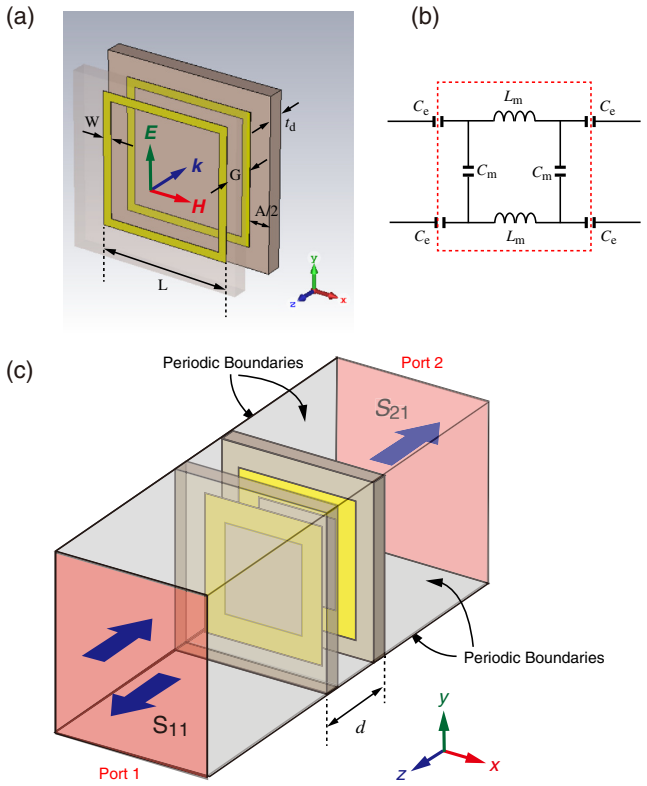


**Fig. 2** Schematic diagram of the analysis model. (a) Unit cell of a double-layered CRR, including definition of the parameters (see Table 1) and direction and polarization of incident EM wave. The front substrate is omitted for clarity. (b) Effective circuit model of the unit cell of double-layered CRR arrays. (c) Unit cell model with periodic boundary conditions.

of aluminum ($t_{Al}$) is 200 nm and its conductivity is $3.56 \times 10^7$ S/cm. The thickness of the quartz substrate ($t_d$) is 10 $\mu$m and its dielectric constant is 3.75. Two such substrates with CRR arrays are placed closely with the gap $G$ of 22 $\mu$m making both of CRR arrays side face inside. The geometric parameters of CRR array are summarized in Table 1.

In our simulation, the EM wave is incident from the normal direction. In such a situation, the resonant modes between the two sides of the paired CRRs with gap $G$ and the near-field coupling between adjacent CRRs on the same substrate can be excited at their resonant frequency. These resonant modes can be approximately modeled by a composite LC-resonance circuit, as shown in Fig. 2(b). The effective values of capacitance and inductance of such an LC circuit are quite sensitive to the geometrical parameters of the CRR array. Therefore, slight displacement of the relative position of CRR arrays and change of the dielectric constant of the dielectrics

**Table 1** Geometric parameters of double-layered CRR arrays.

| Geometric parameters | Values |
|---|---|
| Closed-ring side length: $L$ ($\mu$m) | 80 |
| Closed-ring side width: $W$ ($\mu$m) | 5 |
| Metal thickness: $t_{Al}$ (nm) | 200 |
| Spacing between CRRs: $A$ ($\mu$m) | 25 |
| Gap between CRR arrays: $G$ ($\mu$m) | 22 |
| Substrate thickness: $t_d$ ($\mu$m) | 10 |

inserted between CRR arrays mainly alter effective capacitance, and thus our operative principle is possible.

### 2.2 *Numerical Simulation*

To model the periodic array of CRR, periodic boundary conditions are applied in two ($x$ and $y$) directions, as schematically shown in Fig. 2(c). THz plane waves, whose electric and magnetic fields are uniform over the unit cell and polarized in $y$ and $x$ directions, respectively, are sent to the device from one port in normal ($z$) direction to the CRR arrays and we evaluate the transmission and reflection coefficients (or complex scattering parameters $S_{21}$ and $S_{11}$), as shown in Fig. 2(c).

As discussed above, the resonant response of our device is quite sensitive to the geometric parameters. We examined modulation of the resonant responses by changing the lateral shift of relative position of the double-layered CRR arrays. The initial arrangement where CRR arrays on opposing substrates overlap with no relative displacement looking from normal direction is the defined origin ($\Delta x = \Delta y = 0$ $\mu$m). One of the arrays was laterally moved up to 25 $\mu$m in either $x$ or $y$ direction and resonant responses were evaluated. Tuning of resonant responses of layered-metamaterials by lateral shift in micrometer range was experimentally demonstrated,[22,23] therefore, our models are experimentally feasible. We also examined the modulation of the resonant responses by changing the dielectric constant of the dielectric spacer layer ($\varepsilon_d$) inserted between the double-layered CRR arrays from 2.0 to 4.0 assuming the insertion of organic functional materials.

### 2.3 *Parameter Retrieval*

The impedance $Z$ and refractive index $n$ of a metamaterial slab can be retrieved from its complex transmission ($S_{21}$) and reflection ($S_{11}$) coefficients.[33,34] The impedance $Z$ for normal incidence is expressed as a function of scattering parameters $S_{11}$ and $S_{21}$:

$$Z = \sqrt{\frac{(1+S_{11})^2 - S_{21}^2}{(1-S_{11})^2 - S_{21}^2}}. \tag{1}$$

The refractive index $n$ of a homogeneous passive slab with thickness $d$ is

$$n = -\frac{i}{kd}\ln\left(\frac{S_{21}}{1 - S_{11}\frac{Z-1}{Z+1}}\right), \tag{2}$$

where $k$ is wave number for free space. Since the slab material is passive, the real part of $Z$ and the imaginary part of $n$ should be chosen to be positive. The measure of loss of the slab, figure of merit (FOM), was also evaluated by FOM $= |n_r/n_i|$ from real ($n_r$) and imaginary ($n_i$) parts of refractive indices.

## 3 Results and Discussions

### 3.1 *Index-Tuning by Shifting the Relative Position of the Double-Layered Closed-Ring Resonator Arrays*

A single-layer CRR array may have a relatively wide stop band, as shown in dotted lines in Fig. 3(a). On the contrary, a relatively narrow transmission peak appears within the stop band at around 0.69 THz in a double-layered structure with no displacement ($\Delta x = \Delta y = 0$ $\mu$m), as can be seen in solid lines in Fig. 3(a). The resonant frequency of this transmission peak can be adjusted to particular frequency of interest by modifying the side length $L$ and width $W$ of each CRR accordingly by a scaling rule.[25–27] It is clarified by Gu et al.[27] that this narrow line transmission peak is attributed to two factors, the magnetic response at the two sides of the closest stacked CRR pair spaced by $G$, and the near-field interaction between adjacent CRRs separated by $A$ in the same array. In Fig. 3(c), 3-D plots of the simulated distribution of the magnetic field at 0.577 and

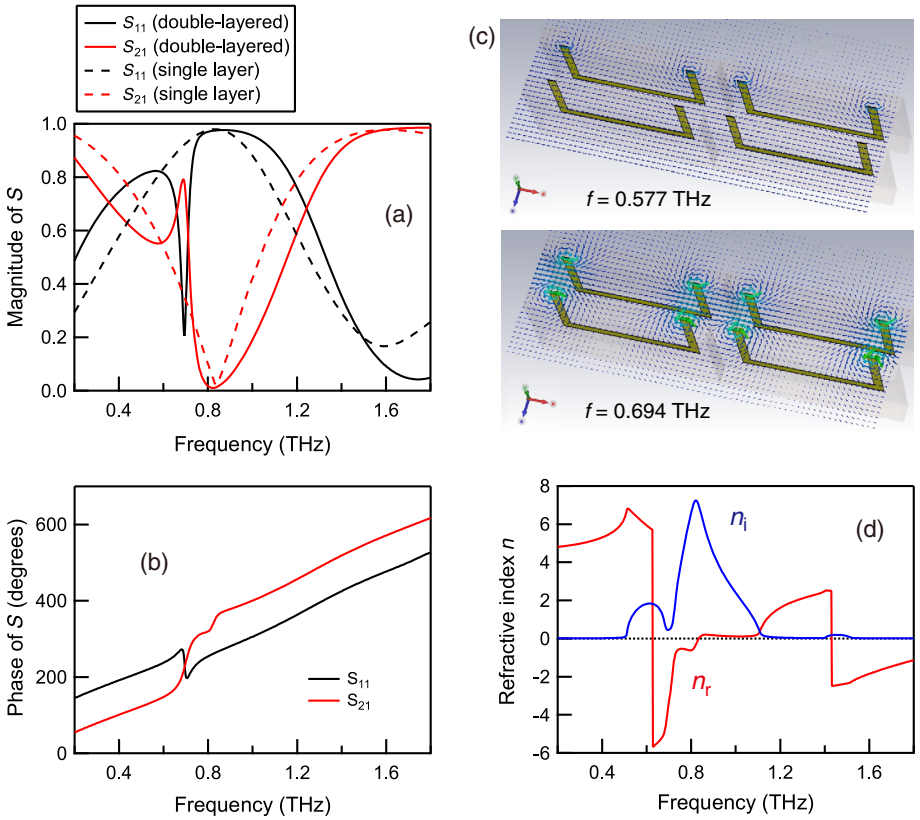


**Fig. 3** Summary of the THz response of double-layered CRR arrays without relative displacement. (a) Magnitude and (b) phase of the simulated scattering parameters $S_{11}$ (reflection) and $S_{21}$ (transmission). (c) Simulated distribution of the magnetic field at 0.577 and 0.694 THz on the cutting plane placed at the middle of each CRRs. (d) Refractive index retrieved from $S_{11}$ and $S_{21}$.

0.694 THz on the cutting plane placed at the middle of each CRRs are shown. It can be visually recognized that closely placed CRRs strongly interact and strong magnetic resonance are induced at around the resonant frequency (0.694 THz). On the contrary, at 0.577 THz, in which the frequency is off from the resonant frequency, only one of the layered CRRs interact with EM wave and show relatively weak resonance. Such resonant responses can be modeled by an equivalent circuit [Fig. 2(b)]. The magnetic response is modeled by a microstrip loop across the two sides of the opposing CRRs. The near-field interaction is modeled by a coplanar line loop across adjacent CRRs in the same array. We previously reported that these resonant responses were quite sensitive to the geometric parameters of the CRR array and showed tuning capability of resonant frequency by giving relative displacement to the CRR arrays or changing dielectric constant of dielectric spacer layer inserted between CRR arrays.[25,26] Here, we further show that the effective refractive index can also be tuned by similar procedures. Figure 3(d) summarizes the effective refractive index of the double-layered CRR array retrieved from complex scattering parameters $S_{21}$ and $S_{11}$ shown in Figs. 3(a) and 3(b). At around narrow band resonant transmission peak, negative index of refraction is observed, similar to a previous report.[27] In the following, we focus on the change in the effective indices by giving relative displacement to the CRR arrays or changing dielectric constant of dielectric media inserted between CRR arrays.

By giving lateral displacement to one of the double-layered CRR arrays in the $x$ direction, the narrow-line resonant transmission peak monotonically shifted to lower frequency, as summarized in Figs. 4(a) and 4(b). The frequency shift reached 17.5 GHz for $\Delta x = 25$ $\mu$m. In Figs. 4(c) and 4(d), 3-D plots of the simulated distribution of the magnetic field at 0.577 and 0.694 THz on the cutting plane placed at the middle of each CRRs are shown. The obtained responses are quite similar to those shown in Fig. 3(c), in which no lateral displacement was given to the layered CRRs. This implies that the basic principle of interaction with EM waves is

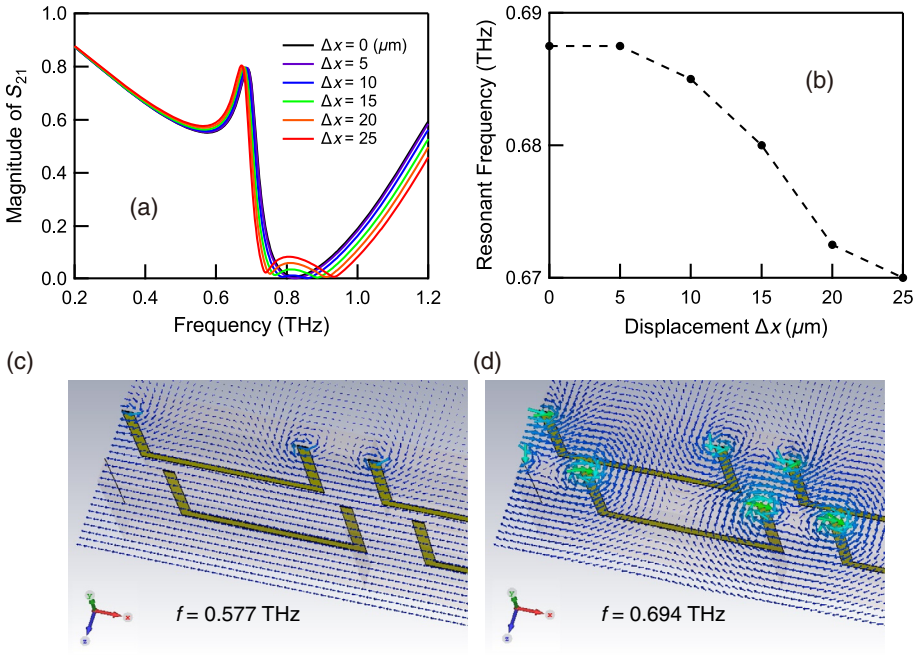


**Fig. 4** Summary of the THz response of double-layered CRR arrays with relative displacement $\Delta x$. (a) Transmission spectra of double-layered CRR arrays with relative displacement $\Delta x$. (b) Relative displacement $\Delta x$ dependence of resonant transmission peak frequency of double-layered CRR arrays. (c) and (d) Simulated distribution of the magnetic field at 0.577 and 0.694 THz on the cutting plane placed at the middle of each CRRs.

unchanged under slight displacement of relative position of CRRs. This can also be understood by the fact that the overall spectral shape does not largely change and slight shift of resonant frequency is obtained.

By introducing a lateral displacement, the effective refractive index can also be tuned. Figures 5(a) and 5(b) summarize the real and imaginary part of the retrieved effective refractive indices, $n_r$ and $n_i$, respectively, for each relative displacement $\Delta x$ as a heat map. It can be seen that the refractive index greatly changes from a positive to a negative value at around 0.6 THz. Above 0.7 THz, the refractive index is small and near zero. For $\Delta x$ larger than 5 $\mu$m, however, the value of the refractive index increases either positive or negative at around 0.8 THz. Figures 5(c) and 5(d) summarize the change in the real part of refractive index ($n_r$) and FOM, respectively, with respect to the displacement of the relative position $\Delta x$ at several frequencies of 0.6250, 0.7050, 0.8025, and 0.8325 THz. These results imply that various ways of tuning of the refractive index can be realized. At 0.6250 THz, the refractive index abruptly changes from a positive high value of $\sim$5.7 to a negative value of approximately $-5.7$ for $\Delta x = 2$ $\mu$m and keeps almost the same value for lager $\Delta x$. The FOM keeps moderately high value of $\sim$3. At 0.7050 THz, the refractive index shows negative value and its absolute value continuously decreases; the refractive index changes from $-2.9$ to $-1.2$ by increasing the relative displacement $\Delta x$ up to 25 $\mu$m. The FOM shows a high value of 5.8 for $\Delta x = 0$, however, continuously decreases by increasing $\Delta x$. At 0.8025 THz, the refractive index similarly shows a negative value but shows opposite trend, that is, its absolute value continuously increases; the refractive index changes from $-0.6$ to $-4.4$ by increasing $\Delta x$ up to 25 $\mu$m. When $\Delta x$ is between 5 and 10 $\mu$m, relatively steep change in the refractive index can be obtained. The FOM, however, shows a low value. At 0.8325 THz, near zero index can be achieved for $\Delta x$ smaller than 6 $\mu$m, and abruptly changes to a positive high value of $\sim$4.0 at $\Delta x = 7$ $\mu$m and keeps almost the same value for $\Delta x$ up to 25 $\mu$m. The FOM is low. These varieties of index-tuning capabilities in the double-layered CRR arrays can be utilized to develop various types of THz optical materials, components, and devices.

We have also investigated similar relative displacement dependence, giving lateral displacement in $y$-direction. In this case, the narrow-line resonant transmission peak monotonically

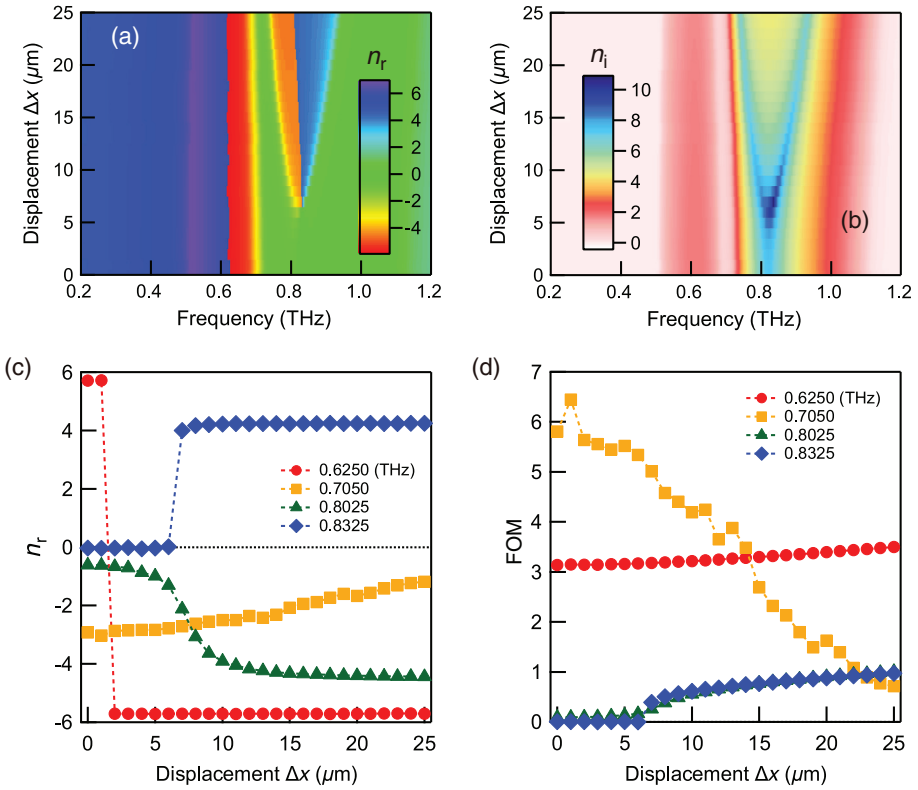


**Fig. 5** Summary of relative displacement $\Delta x$ dependence of the effective refractive indices. The heat maps represent the change in (a) real and (b) imaginary part of the refractive index with respect to the relative displacement $\Delta x$. Summary of relative displacement $\Delta x$ dependence of (c) real part of the refractive index and (d) FOM of double-layered CRR arrays at specific frequencies of 0.6250, 0.7050, 0.8025, and 0.8325 THz.

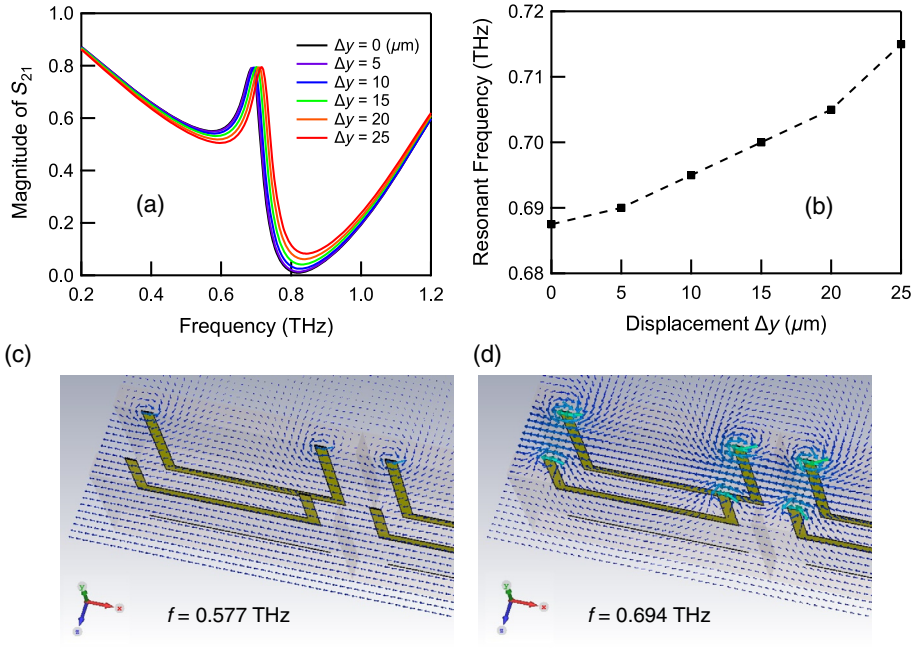


**Fig. 6** Summary of the THz response of double-layered CRR arrays with relative displacement $\Delta y$. (a) Transmission spectra of double-layered CRR arrays with relative displacement $\Delta y$. (b) Relative displacement $\Delta y$ dependence of resonant transmission peak frequency of double-layered CRR arrays. (c) and (d) Simulated distribution of the magnetic field at 0.577 and 0.694 THz on the cutting plane placed at the middle of each CRRs.

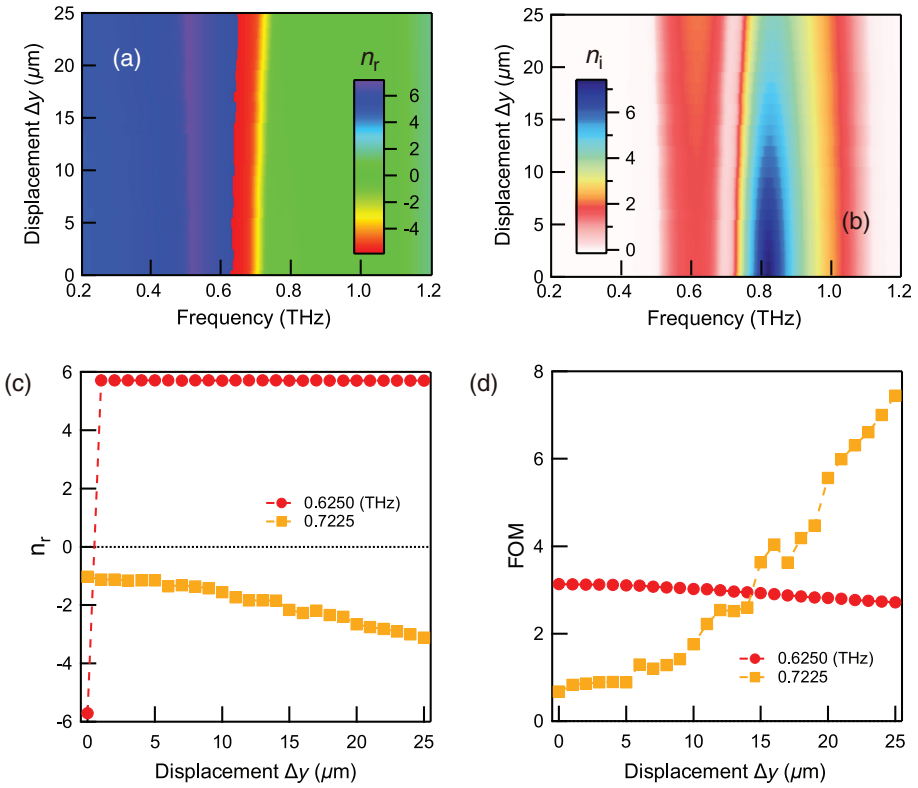


**Fig. 7** Summary of relative displacement $\Delta y$ dependence of the effective refractive indices. The heat maps represent the change in (a) real and (b) imaginary part of the refractive index with respect to the relative displacement $\Delta y$. Summary of relative displacement $\Delta y$ dependence of (c) real part of the refractive index and (d) FOM of double-layered CRR arrays at specific frequencies of 0.6250 and 0.7225 THz.

shifted to the opposite direction, to a higher frequency, as summarized in Figs. 6(a) and 6(b). The amount of frequency shift is larger and reached 27.5 GHz for $\Delta y = 25$ $\mu$m. Therefore, in our device, the resonance frequency can be shifted to both lower and higher frequency according to the direction of the relative displacement ($\Delta x$, $\Delta y$) given to the double-layered CRR arrays.[25,26] In Figs. 6(c) and 6(d), 3-D plots of the simulated distribution of the magnetic field at 0.577 and 0.694 THz on the cutting plane placed at the middle of each CRRs are shown. The obtained responses in this case are also similar to those shown in Figs. 3(c), 4(c), and 4(d).

The heat maps in Figs. 7(a) and 7(b) show real and imaginary part of the retrieved effective refractive index, $n_r$ and $n_i$, respectively, for each relative displacement $\Delta y$. It can be seen that the band around 0.6 to 0.7 THz in which the refractive index shows negative value shifts to higher frequency together with a narrow-line resonant transmission peak by increasing $\Delta y$. Figures 7(c) and 7(d) summarize the change in the real part of the refractive index ($n_r$) and FOM, respectively, with respect to the displacement of the relative position $\Delta y$ at 0.6250 and 0.7225 THz. At 0.6250 THz, the refractive index shows a negative high value of $-5.7$ for $\Delta y = 0$ and abruptly changes to a positive high value of 5.7 by giving small displacement $\Delta y$ of only 1 $\mu$m and almost unchanged for $\Delta y$ up to 25 $\mu$m. The FOM keeps a moderately high value of $\sim$3. At 0.7225 THz, the refractive index shows a negative value, and its absolute value continuously increases; the refractive index changes from $-1.0$ to $-3.1$ by increasing the relative displacement $\Delta y$ up to 25 $\mu$m. The FOM continuously increases by increasing $\Delta y$.

## 3.2 *Index-Tuning by Changing the Dielectric Constant of the Dielectric Media Inserted Between the Double-Layered Closed-Ring Resonator Arrays*

We have also investigated the index-tuning capability of the double-layered CRR arrays by changing the dielectric constant $\varepsilon_d$ of spacer inserted between the double-layered CRR arrays.

In this case, no lateral displacement was given to the arrays ($\Delta x = \Delta y = 0$). The narrow-line resonant transmission peak monotonically shifted to lower frequency by changing the dielectric constant $\varepsilon_d$ from 2.0 to 4.0, as shown in Figs. 8(a) and 8(b). The resonant frequency shifted by 110 GHz. The heat maps in Figs. 8(c) and 8(d) show real and imaginary part of the retrieved effective refractive index, $n_r$ and $n_i$, respectively, for each dielectric constant $\varepsilon_d$. In comparison with the index-tuning by giving the relative displacement $(\Delta x, \Delta y)$, the change in the effective refractive index due to the change in the dielectric constant $\varepsilon_d$ is remarkable. Figures 8(e) and 8(f) summarize the change in the real part of the refractive index ($n_r$) and FOM, respectively, with respect to the dielectric constant $\varepsilon_d$ of a dielectrics inserted between the double-layered CRR arrays at 0.5075, 0.5650, and 0.6500 THz. At 0.5075 THz, the refractive index shows a positive high value of ~7.0 for $\varepsilon_d$ less than 2.6 and abruptly changes its sign to negative

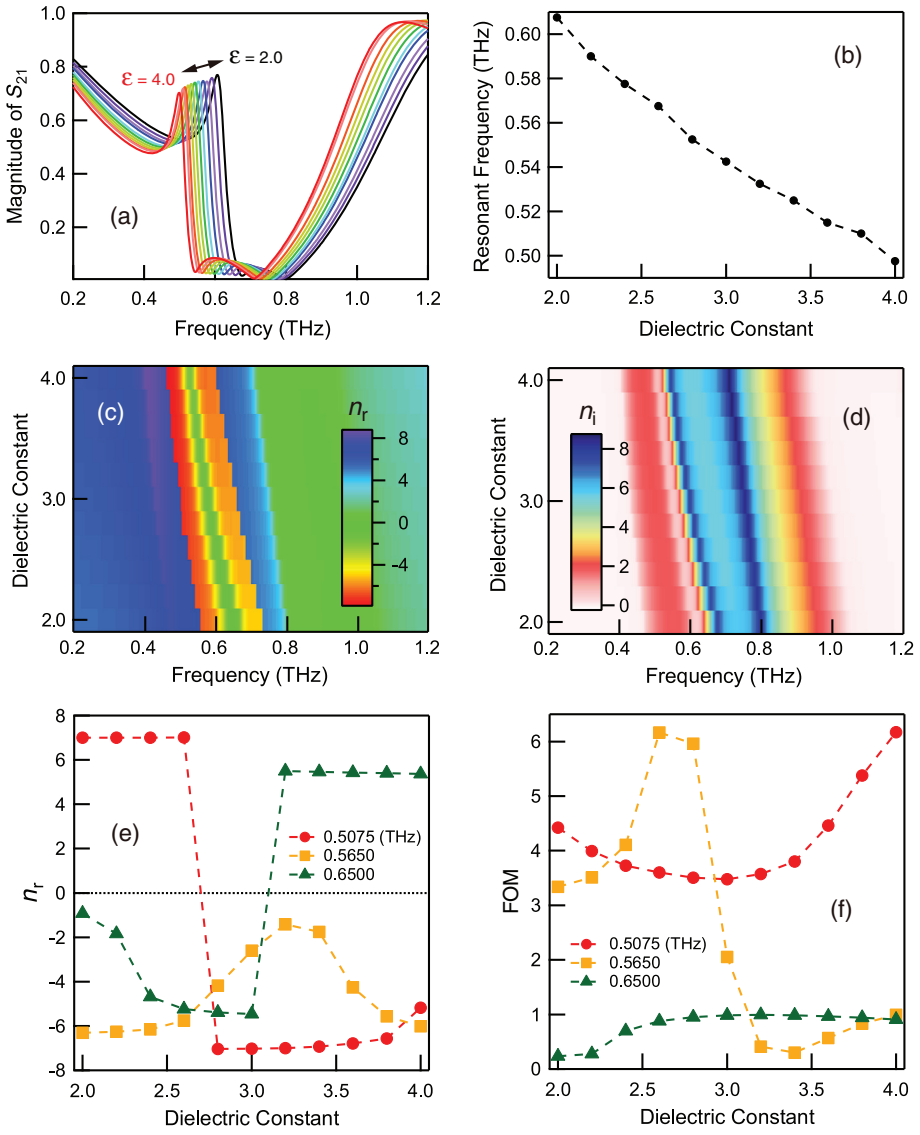


**Fig. 8** Summary of the THz response of double-layered CRR arrays by changing the dielectric constant $\varepsilon_d$ of dielectric spacer inserted between double-layered CRR arrays. (a) Transmission spectra of double-layered CRR arrays for several values of dielectric constant $\varepsilon_d$. (b) Transmission peak frequency of double-layered CRR arrays as a function of dielectric constant $\varepsilon_d$. Heat maps represent the change in (c) real and (d) imaginary part of the refractive index as a function of dielectric constant $\varepsilon_d$. Summary of (e) real part of the refractive index and (f) FOM of double-layered CRR arrays at specific frequencies of 0.5075, 0.5650, and 0.6500 THz as a function of the dielectric constant $\varepsilon_d$ of dielectric inserted between double-layered CRR arrays.

and keeps almost the same value of −7.0 by further increasing $\varepsilon_d$. The FOM keeps a moderately high value, larger than ∼3.5. At 0.5650 THz; the refractive index shows a negative value, and its absolute value continuously decreased; the refractive index changes from −6.3 to −1.4 by increasing the dielectric constant $\varepsilon_d$ of the dielectric from 2.0 to 3.2, however, returned to almost the same value by further increasing $\varepsilon_d$ up to 4.0. The FOM shows moderately high value for $\varepsilon_d$ less than 3.0, however, drops to less than 1 by further increasing $\varepsilon_d$. At 0.6500 THz, the refractive index shows negative value, and its absolute value increased; the refractive index changes from −0.9 to −5.5 by increasing the dielectric constant $\varepsilon_d$ of the dielectric from 2.0 to 3.0, however, abruptly changes its sign to positive and keeps almost the same value of ∼5.4 by further increasing the dielectric constant $\varepsilon_d$. The FOM is low. Changing the refractive index of dielectrics does not require mechanical displacement of the layers and can be more easily implemented by liquid crystals, etc.

## 4 Conclusions

In conclusion, we have numerically investigated index-tuning properties of double-layered CRR arrays operating in the THz frequency range. Double-layered CRR arrays have a narrow-band transmission peak in a relatively wide stop band. The position of that peak can be shifted to lower or higher frequencies by slightly shifting the relative position of the arrays perpendicular to the polarization direction of the incident EM wave or parallel to it. The effective refractive index can also be tuned by adjusting relative displacement. Such index-tuning can be done in various ways, continuously or stepwise, from positive to negative or oppositely, etc. We also demonstrate that spectral shift and index-tuning can be done by changing dielectric constant of the dielectric media inserted between CRR arrays. Our approach may be utilized to develop the type of THz active devices.

## Acknowledgments

This work is partly supported by Strategic Information and Communications R&D Promotion Program (SCOPE) from the Ministry of Internal Affairs and Communications of Japan.

## References

1. M. Tonouchi, "Cutting-edge terahertz technology," *Nat. Photonics* **1**(2), 97–105 (2007).
2. M. Hangyo, "Development and future prospects of terahertz technology," *Jpn. J. Appl. Phys.* **54**(12), 120101 (2015).
3. M. Rahm, J.-S. Li, and W. J. Padilla, "THz wave modulators: a brief review on different modulation techniques," *J. Infrared Millimeter Terahertz Waves* **34**, 1–27 (2013).
4. I. Al-Naib and W. Withayachumnankul, "Recent progress in terahertz metasurfaces," *J. Infrared Millimeter Terahertz Waves* **38**, 1067–1084 (2017).
5. V. M. Shalaev, "Optical negative-index meta- materials," *Nat. Photonics* **1**, 41–48 (2007).
6. C. M. Soukoulis and M. Wegener, "Past achievements and future challenges in the development of three-dimensional photonic metamaterials," *Nat. Photonics* **5**, 523–530 (2011).
7. N. I. Zheludev and Y. S. Kivshar, "From metamaterials to metadevices," *Nat. Mater.* **11**(11), 917–924 (2012).
8. R. A. Shelby, D. R. Smith, and S. Schultz, "Experimental verification of a negative index of refraction," *Science* **292**, 77–79 (2001).
9. J. B. Pendry, "Negative refraction makes a perfect lens," *Phys. Rev. Lett.* **85**, 3966–3969 (2000).
10. N. Fang et al., "Sub-diffraction-limited optical imaging with a silver superlens," *Science* **308**, 534–537 (2005).
11. Z. Liu et al., "Far-field optical hyperlens magnifying sub-diffraction-limited objects," *Science* **315**, 1686–1686 (2007).
12. J. B. Pendry et al., "Magnetism from conductors, and enhanced non-linear phenomena," *IEEE Trans. Microwave Theory Tech.* **47**(11), 2075–2084 (1999).

13. M. Lapine et al., "Structural tunability in metamaterials," *Appl. Phys. Lett.* **95**, 084105 (2009).
14. H. Liu et al., "Coupled magnetic plasmons in metamaterials," *Phys. Status Solidi B* **246**, 1397–1406 (2009).
15. D. A. Powell et al., "Metamaterial tuning by manipulation of near-field interaction," *Phys. Rev. B* **82**(15), 155128 (2010).
16. E. Ekmekci et al., "Frequency tunable terahertz metamaterials using broadside coupled split-ring resonators," *Phys. Rev. B* **83**(19), 193103 (2011).
17. D. A. Powell et al., "Near-field interaction of twisted split-ring resonators," *Phys. Rev. B* **83**(23), 235420 (2011).
18. M. Lapine et al., "Magnetoelastic metamaterials," *Nat. Mater.* **11**, 30–33 (2012).
19. M. Liu et al., "Nonlinear response via intrinsic rotation in metamaterials," *Phys. Rev. B* **87**(23), 235126 (2013).
20. T. Matsui et al., "Electromagnetic tuning of resonant transmission in magnetoelastic metamaterials," *Appl. Phys. Lett.* **104**(16), 161117 (2014).
21. L. Liu et al., "Post-processing approach for tuning multi-layered metamaterials," *Appl. Phys. Lett.* **105**(15), 151102 (2014).
22. T. Matsui et al., "Electroactive tuning of double-layered metamaterials based on π-conjugated polymer actuators," *Adv. Opt. Mater.* **4**, 135–140 (2016).
23. X. Zhao et al., "Voltage-tunable dual-layer terahertz metamaterials," *Microsys. Nanoeng.* **2**, 16025 (2016).
24. P. Pitchappa et al., "Bidirectional reconfiguration and thermal tuning of microcantilever metamaterial device operating from 77 K to 400 K," *Appl. Phys. Lett.* **111**(26), 261101 (2017)
25. T. Matsui, S. Asano, and H. Mori, "Terahertz active metamaterials based on stacked closed-ring resonator arrays," *IEEJ Trans. Sens. Micromach.* **137**(11), 371–378 (in Japanese) (2017).
26. T. Matsui, S. Asano, and H. Mori, "Terahertz active metamaterials based on stacked closed-ring resonator arrays," *Electr. Eng. Jpn.* **203**(3), 56–65 (2018) (English translation of Ref. 25).
27. J. Gu et al., "A close-ring pair terahertz metamaterial resonating at normal incidence," *Opt. Express* **17**(22), 20307–20312 (2009).
28. M. Choi et al., "A terahertz metamaterial with unnaturally high refractive index," *Nature* **470**, 369–373 (2011).
29. K. Ishihara and T. Suzuki, "Metamaterial demonstrates both a high refractive index and extremely low reflection in the 0.3-THz Band," *J. Infrared Millimeter Terahertz Waves* **38**(9), 1130–1139 (2017).
30. L. Singh, R. Singh, and W. Zhang, "Ultra-high terahertz index in deep subwavelength coupled bi-layer free-standing flexible metamaterials," *J. Appl. Phys.* **121**(23), 233103 (2017).
31. M. Silveirinha and N. Engheta, "Tunneling of electromagnetic energy through subwavelength channels and bends using $\varepsilon$-near-zero materials," *Phys. Rev. Lett.* **97**(15), 157403 (2006).
32. I. Liberal and N. Engheta, "Near-zero refractive index photonics," *Nat. Photonics* **11**, 149–158 (2017).
33. D. R. Smith et al., "Determination of effective permittivity and permeability of metamaterials from reflection and transmission coefficients," *Phys. Rev. B* **65**, 195104 (2002).
34. X. Chen et al., "Robust method to retrieve the constitutive effective parameters of metamaterials," *Phys. Rev. E* **70**, 016608 (2004).

**Yuki Watanabe** was graduated from the Department of Electrical and Electronic Engineering, faculty of engineering, Mie University, in March 2017. Currently, he is at the same department of the Graduate School of Engineering of Mie University pursuing his master's degree. He is engaged in research on THz metamaterials.

**Tatsunosuke Matsui** is an associate professor at Department of Electrical and Electronic Engineering of Mie University, Japan. He received his BS, MS, and PhD degrees in electronic engineering from Osaka University in 1999, 2001, and 2004, respectively. From 2004, he worked in the Physics Department of the University of Utah as a postdoctoral researcher for three years. In March 2007, he joined Mie University as a faculty. His current research interests include plasmonics, metamaterials, and THz technology.